

Composition of a plasma generated from N_2-O_2 by an Ar ion jet in a low pressure reactor

This article has been downloaded from IOPscience. Please scroll down to see the full text article.

2010 J. Phys. D: Appl. Phys. 43 055201

(<http://iopscience.iop.org/0022-3727/43/5/055201>)

[The Table of Contents](#) and [more related content](#) is available

Download details:

IP Address: 148.6.27.69

The article was downloaded on 27/01/2010 at 13:48

Please note that [terms and conditions apply](#).

Composition of a plasma generated from N₂–O₂ by an Ar ion jet in a low pressure reactor

Kinga Kutasi

Research Institute for Solid State Physics and Optics, Hungarian Academy of Sciences, POB 49, H-1525 Budapest, Hungary

E-mail: kutasi@sunserv.kfki.hu

Received 4 September 2009, in final form 16 November 2009

Published 21 January 2010

Online at stacks.iop.org/JPhysD/43/055201

Abstract

The expansion of a supersonic Ar⁺ ion jet in a low pressure (0.2 Torr) reactor filled with N₂ and O₂ has been investigated by means of hydrodynamic modelling. The gas velocity fields and the gas temperature distribution in the three-dimensional reactor have been determined. The formation of different species through the molecular kinetics triggered by the collision of Ar⁺ ions with N₂ and O₂ molecules has been studied. We have investigated the effect of the ions velocity and molecular gas flow rates on the gas temperature and species density distributions. We have shown that the main difference between this system and an N₂–O₂ post-discharge lies in the dissociation degrees of N₂ and O₂. While in an N₂–O₂ post-discharge the N₂ dissociation degree is low and that of O₂ is high, in the present system this can be varied through the gas flow rate of the molecular gases. We have also shown that the NO(*X*) molecules formation is governed by the surface processes, which is strongly influenced by the state of the surface.

1. Introduction

Low pressure plasmas that contain N and O atoms and excited NO molecules have a wide range of applications, such as metal surface cleaning [1], medical sterilization [2, 3], etching and grafting of polymers [4, 5], silicon oxidation [6], thin film synthesis [7], to increase surface adhesion [8] and textile material modification [9]. In numerous cases instead of the active discharge region the remote post-discharge is used, where the density of charge species is negligible.

In N₂ or N₂–O₂ discharges usually low N₂ dissociation degree can be achieved, e.g. in low pressure N₂–O₂ surface wave discharges depending on frequency and discharge tube radius the dissociation degree can be a few per cent [10–12], which further decreases in the afterglow due to the N atoms recombination. In N₂–O₂ systems, which are successfully used for plasma sterilization, the formation of UV emitting excited NO(*A*, *B*) molecules through the N and O atoms association process in the afterglow is limited by the N atoms density, the N₂ being less dissociated than the O₂ [13, 14]. However, in the expanding thermal plasma (ETP) presented

by van Helden *et al* [15] higher N₂ dissociation degrees may be achieved outside the active discharge region. The ETP consists of a high-pressure thermal plasma, here namely a dc cascaded Ar arc discharge, and a low pressure process chamber, where the molecular gases to be dissociated are injected. The large pressure difference between the cascaded arc source (40 kPa) and the process chamber (typically 20–100 Pa) causes a supersonic expansion of the plasma from the nozzle of the cascaded arc into the chamber. The high velocity ($\approx 2000 \text{ m s}^{-1}$) Ar ions so introduced into the vessel can strongly dissociate the N₂–O₂ molecules.

van Helden *et al* [15] have conducted mass spectrometry measurements on Ar–N₂–O₂ ETP. The mass spectra were measured by sampling the gas through a controlled all-metal regulating valve connected to the reactor through a metal tube. With this method the absolute concentrations of the stable gas species N₂, O₂ and NO were determined. Here, no atomic species have been detected; however, they are present in the reactor, but they are likely to recombine on the way to the spectrometer unit. Zijlman *et al* [16] have developed a model in order to reveal the creation mechanisms of the stable molecules detected.

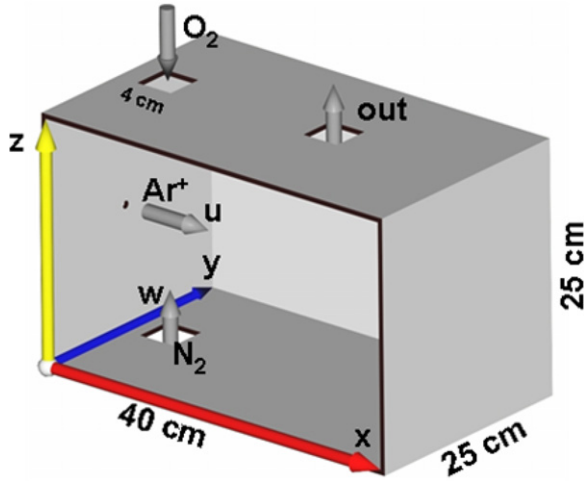


Figure 1. Structure of the 40 cm × 25 cm × 25 cm parallelepipedic reactor. The reactor has three inlets as follows: (i) a 4 × 4 mm² square inlet on the left side plate, (ii) a 4 × 4 cm² inlet on the top plate and (iii) a 4 × 4 cm² inlet on the bottom plate. The 4 × 4 cm² gas outlet is positioned on the top plate.

(This figure is in colour only in the electronic version)

The aim of this work is to give a detailed description of a low pressure reactor, where the plasma is sustained in N₂–O₂ by the externally generated Ar ion jet. Therefore, we determine the expansion of the plasma in the reactor under the effect of different—Ar ion and molecular gas—flows, as well as the spatial distribution of the density of different species created in the reactor. Further, we investigate the formation of the toxic NO molecules, both in the gas phase and on the stainless steel walls of the reactor.

2. System set-up

The system investigated in this work has a similar structure as that of van de Sanden *et al* [18] and van Helden *et al* [15]. Here the plasma reactor is a parallelepipedic stainless steel chamber with dimensions of 40 cm × 25 cm × 25 cm (*x*, *y*, *z*). The 4 × 4 mm² square inlet, where the high velocity—2000 m s⁻¹ according to Engeln *et al* [17]—Ar⁺ ions from the dc cascaded arc source enter the reactor, is located in the middle of the left plate, while the 4 × 4 cm² gas outlet of the top plate, as it is shown in figure 1. Two more inlets of 4 × 4 cm², which serve as inlets for the molecular gases, are located on the bottom and top plates, respectively, at about 2 cm from the left plate.

3. The hydrodynamic model

The expansion of a supersonic cascaded arc plasma into a low pressure atmosphere has been studied by Selezneva *et al* [19] with the help of two computational approaches: the continuum fluid dynamics and direct simulation Monte Carlo. They have shown that the velocity and temperature profiles in the reactor are very well predicted by the two-dimensional FLUENT model when the pressure in the chamber is 0.15 Torr. Therefore, we find a three-dimensional

hydrodynamic model to be feasible for the description of the plasma generated 0.2 Torr in the reactor by the high velocity Ar⁺ jet produced in the external cascaded arc source (not modelled here).

The three-dimensional hydrodynamic model developed by us is composed of (i) the total mass conservation, (ii) the continuity equations for the different species (2), (iii) the total momentum conservation equation (3) and (iv) the total energy conservation equation (4). The gas is assumed to be a Newtonian fluid. The continuity equations can be written in the following form when the Soret and pressure diffusions are neglected, as well as the Dufour effect [14]:

$$\int_S \rho \mathbf{v} \cdot \mathbf{n} dS = 0, \quad (1)$$

$$\begin{aligned} \int_S \rho y_k \mathbf{v} \cdot \mathbf{n} dS - \int_S \nabla(D_k \rho y_k) \cdot \mathbf{n} dS \\ = \int_V m_k S_k^V dV + \int_S m_k S_k^S dS, \end{aligned} \quad (2)$$

$$\int_S \rho u_i \mathbf{v} \cdot \mathbf{n} dS = \int_S \mu \text{grad } u_i \cdot \mathbf{n} dS - \int_S p i_i \cdot \mathbf{n} dS, \quad (3)$$

$$\int_S \rho T \mathbf{v} \cdot \mathbf{n} dS = \int_S \frac{\lambda}{C_p} \text{grad } T \cdot \mathbf{n} dS. \quad (4)$$

Here ρ denotes the total gas density (mass density), \mathbf{v} the gas velocity and \mathbf{n} the unit vector orthogonal to the S surface and directed outwards. Further, y_k denotes the relative mass density ($y_k = \rho_k/\rho$), D_k and m_k are the diffusion coefficient and the mass of the species k , and S_k^V and S_k^S represent the source terms associated with volume and surface reactions, respectively. Since S_k^S represents a term taking into account surface losses, this term is considered in (2) only on the last grid point at the proximity of the surface. u_i is the velocity in the i direction, p the static pressure, μ the dynamic viscosity, T is the gas temperature, C_p the specific heat at constant pressure and λ the thermal conductivity. The transport data values for the N and O containing species are taken from [20], while for the Ar atom from [21].

The term S_k^V is the sum of the source terms associated with the various gas phase reactions [14]. A list of gas phase reactions for neutral species taken into account in the model is given in tables 1 and 2. The neutral species kinetics in the reactor starts up with the creation of the active atoms, namely N and O atoms. The N and O atoms in the reactor can be created through the following reactions: Ar⁺ + N₂ → Ar + N₂⁺ (4.45 × 10⁻¹⁶ m³ s⁻¹ [22]), N₂⁺ + e → N + N (2 × 10⁻¹³ m³ s⁻¹ [15]) and Ar⁺ + O₂ → Ar + O₂⁺ (4.9 × 10⁻¹⁷ (300/ T)^{0.78} + 9.2 × 10⁻¹⁶ exp(-5027.6/ T) m³ s⁻¹ [23]), O₂⁺ + e → O + O (2 × 10⁻¹³ m³ s⁻¹ [15]), respectively. In order to simplify our model we do not follow the electrons, which in fact are low energy electrons with $T_e = 0.1$ – 0.3 eV, as reported in [15, 18], thus these electrons do not play an important role in the excitation and ionization kinetics, they are involved only in the recombination processes. The electron dissociative recombination of molecular ions, created in the charge transfer reaction presented above, is very fast and has the same rate for both O₂⁺ and N₂⁺, therefore we assume that the

Table 1. Reactions taken into account in the hydrodynamic model. The rate coefficients for the reactions of oxygen species are taken from [12, 24], while for those of Ar species from [21]. The rate coefficients for the two- and three-body reactions are in $\text{m}^3 \text{s}^{-1}$ and $\text{m}^6 \text{s}^{-1}$, respectively, and the decay frequencies are in s^{-1} . T is the temperature in Kelvin.

Processes	Rate coefficients
R1. $\text{O}(^3\text{P}) + \text{O}(^3\text{P}) + \text{O}_2 \rightarrow \text{O}_2 + \text{O}_2$	$0.5 \times 3.8 \times 10^{-42} \exp(-170/T)/T$
R2. $\text{O}(^3\text{P}) + \text{O}(^3\text{P}) + \text{O}_2 \rightarrow \text{O}_2(a) + \text{O}_2$	$0.33 \times 3.8 \times 10^{-42} \exp(-170/T)/T$
R3. $\text{O}(^3\text{P}) + \text{O}(^3\text{P}) + \text{O}_2 \rightarrow \text{O}_2(b) + \text{O}_2$	$0.17 \times 3.8 \times 10^{-42} \exp(-170/T)/T$
R4. $\text{O}(^3\text{P}) + \text{O}(^3\text{P}) + \text{O}(^3\text{P}) \rightarrow \text{O}_2 + \text{O}(^3\text{P})$	$3.6 \times 10^{-44} T^{-0.63}$
R5. $\text{O}(^3\text{P}) + \text{O}_2(X) + \text{O}_2 \rightarrow \text{O}_3 + \text{O}_2$	$6.4 \times 10^{-47} \exp(663/T)$
R6. $\text{O}(^3\text{P}) + \text{O}(^3\text{P}) + \text{O}_2 \rightarrow \text{O}_3 + \text{O}(^3\text{P})$	$2.1 \times 10^{-46} \exp(345/T)$
R7. $\text{O}_2(a) + \text{O}_2 \rightarrow \text{O}_2(X) + \text{O}_2$	$2.2 \times 10^{-24} (T/300)^{0.8}$
R8. $\text{O}_2(a) + \text{O}(^3\text{P}) \rightarrow \text{O}_2(X) + \text{O}(^3\text{P})$	7×10^{-22}
R9. $\text{O}_2(a) + \text{O}_3 \rightarrow \text{O}_2(X) + \text{O}_2(X) + \text{O}(^3\text{P})$	$5.2 \times 10^{-17} \exp(-2840/T)$
R10. $\text{O}_3 + \text{O}(^3\text{P}) \rightarrow \text{O}_2(X) + \text{O}_2(X)$	$0.5 \times 1.8 \times 10^{-17} \exp(-2300/T)$
R11. $\text{O}_3 + \text{O}(^3\text{P}) \rightarrow \text{O}_2(a) + \text{O}_2(X)$	$0.33 \times 1.8 \times 10^{-17} \exp(-2300/T)$
R12. $\text{O}_3 + \text{O}(^3\text{P}) \rightarrow \text{O}_2(b) + \text{O}_2(X)$	$0.17 \times 1.8 \times 10^{-17} \exp(-2300/T)$
R13. $\text{O}_2(b) + \text{O}(^3\text{P}) \rightarrow \text{O}_2(X) + \text{O}(^3\text{P})$	4×10^{-20}
R14. $\text{O}_2(b) + \text{O}(^3\text{P}) \rightarrow \text{O}_2(a) + \text{O}(^3\text{P})$	4×10^{-20}
R15. $\text{O}_2(b) + \text{O}_3 \rightarrow \text{O}_2(X) + \text{O}_2(X) + \text{O}(^3\text{P})$	1.5×10^{-17}
R16. $\text{O}(^3\text{P}) + \text{O}_2(X) + \text{O}_3 \rightarrow \text{O}_3 + \text{O}_3$	$1.66 \times 10^{-46} \exp(T/300)$
R17. $\text{O}(^3\text{P}) + \text{O}(^3\text{P}) + \text{Ar} \rightarrow \text{O}_2(X) + \text{Ar}$	$5.21 \times 10^{-47} \exp(900/T)$
R18. $\text{O}_2(b) + \text{Ar} \rightarrow \text{O}_2(X) + \text{Ar}$	1.5×10^{-23}
R19. $\text{O}(^3\text{P}) + \text{O}_2 + \text{Ar} \rightarrow \text{O}_3 + \text{Ar}$	$3.9 \times 10^{-46} (300/T)^{1.9}$
R20. $\text{O}_2(a) + \text{Ar} \rightarrow \text{O}_2(X) + \text{Ar}$	1.5×10^{-26}

collision of Ar^+ ions with N_2 and O_2 result in the dissociation of the molecules (i.e. the molecular dissociation occurs in one step $\text{Ar}^+ + \text{N}_2 \rightarrow [\text{Ar} + \text{N}_2^+, \text{N}_2^+ + e] \rightarrow \text{ArN} + \text{N}$), producing ground state $\text{N}(^4\text{S})$ and $\text{O}(^3\text{P})$ atoms.

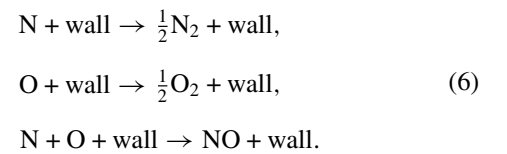
With the appearance of $\text{O}(^3\text{P})$ and $\text{N}(^4\text{S})$ atoms further reactions can take place in the reactor filled with O_2 and N_2 , which give rise to excited and newly formed molecules. First of all, the three-body recombination of $\text{O}(^3\text{P})$ results in excited $\text{O}_2(a)$ (R2) and $\text{O}_2(b)$ (R3) molecules, as well as O_3 (R5, R6, R19), see table 1. The so created molecules are then lost in collisions with $\text{O}(^3\text{P})$ and O_2 (R7–R14). In the case of $\text{N}(^4\text{S})$ atoms, their three-body recombination results in excited $\text{N}_2(B)$ molecules (R21), see table 2. The quenching of $\text{N}_2(B)$ by N_2 (R22) and its radiative decay (R24) results in metastable $\text{N}_2(A)$ molecules, which afterwards are lost through quenching by O_2 (R29–R30) and $\text{O}(^3\text{P})$ (R31). The $\text{N}(^4\text{S})$ atoms further contribute to the formation of ground-state $\text{NO}(X)$ molecules through two-body collision with $\text{O}_2(X)$ (R32) and $\text{O}_2(a)$ (R33), and through three-body re-association process with $\text{O}(^3\text{P})$ in the presence of Ar, N_2 and O_2 (R36). The three-body re-association of $\text{N}(^4\text{S})$ and $\text{O}(^3\text{P})$ atoms also gives rise to excited $\text{NO}(B)$ (R37) and $\text{NO}(A)$ (R38) molecules that are subsequently lost in the reactor mostly through radiative decay (R40, R44) and in smaller part through quenching by N_2 , O_2 and NO , respectively (R41–R43, R45–R47). Further, the NO molecules participate in the destruction of $\text{N}(^4\text{S})$ atoms (R48) and excited O_2 molecules (R49, R50), as well as in the creation of $\text{NO}_2(X)$ (R54–R57) through the three-body re-association with $\text{O}(^3\text{P})$ in the presence of N_2 , O_2 and Ar, respectively. The $\text{NO}_2(X)$ molecules are lost mostly through collisions with $\text{N}(^4\text{S})$ (R58–R60) and $\text{O}(^3\text{P})$ (R61) atoms.

In what concerns the term for the surface losses, the following procedure is used. The term for surface loss of the

atomic species is calculated using the standard procedure

$$S_k^S = -\gamma_k \frac{v_k}{4} n_k, \quad (5)$$

where $v_k = \sqrt{8k_B T / \pi m_k}$ is the average velocity of k atoms and γ_k is the corresponding atomic surface loss probability. The γ surface recombination probability includes all the possible surface reactions, thus making it possible to describe the loss and creation of species on the surface without a detailed surface kinetic model. The losses of atomic species on the wall are attributed to three different elementary processes, which are assumed to be first order [25], and can be written schematically in the form:



Due to the difficulty of knowing, based on the data available in the literature, which is the contribution of each of the above-mentioned mechanisms to the whole surface loss rate of atoms, in the calculation of surface source terms— S_{NO}^S , $S_{\text{N}_2}^S$, $S_{\text{O}_2}^S$ —we introduce an α parameter, with possible values in the 0–1 interval, which defines what percentage of the atoms lost on the surface recombine into NO . In fact, we distinguish two different cases depending on which atomic surface loss is lower. When the N atoms surface loss $|S_{\text{N}}^S|$ is lower than that of O atoms $|S_{\text{O}}^S|$, we assume that α percentage of the N atoms lost on the surface recombine with an equal O atoms concentration forming NO molecules [26], thus the source of NO molecules is $|S_{\text{NO}}^S| = \alpha |S_{\text{N}}^S|$. According to this assumption the loss/source terms of different species on the boundary surface, associated with N and O atoms destruction and with NO , N_2 and O_2

Table 2. Reactions taken into account in the hydrodynamic model. The rate coefficients are taken from [12, 13, 24]. The rate coefficients for the two- and three-body reactions are in $\text{m}^3 \text{s}^{-1}$ and $\text{m}^6 \text{s}^{-1}$, respectively, and the decay frequencies are in s^{-1} . T is the temperature in Kelvin.

Processes	Rate coefficients
R21. $\text{N}(^4\text{S}) + \text{N}(^4\text{S}) + \text{N}_2 \rightarrow \text{N}_2(\text{B}) + \text{N}_2$	$8.27 \times 10^{-46} \exp(T/300)$
R22. $\text{N}_2(\text{B}) + \text{N}_2(\text{X}) \rightarrow \text{N}_2(\text{A}) + \text{N}_2(\text{X})$	$0.95 \times 3 \times 10^{-17}$
R23. $\text{N}_2(\text{B}) + \text{N}_2(\text{X}) \rightarrow \text{N}_2(\text{X}) + \text{N}_2(\text{X})$	$0.05 \times 3 \times 10^{-17}$
R24. $\text{N}_2(\text{B}) \rightarrow \text{N}_2(\text{A}) + h\nu$	2×10^5
R25. $\text{N}_2(\text{B}) + \text{O}_2 \rightarrow \text{N}_2(\text{X}) + \text{O}(^3\text{P}) + \text{O}(^3\text{P})$	3×10^{-16}
R26. $\text{N}_2(\text{A}) + \text{O}(^3\text{P}) \rightarrow \text{NO}(\text{X}) + \text{N}(^2\text{D})$	7×10^{-18}
R27. $\text{N}_2(\text{A}) + \text{N}_2(\text{A}) \rightarrow \text{N}_2(\text{B}) + \text{N}_2(\text{X})$	7.7×10^{-17}
R28. $\text{N}_2(\text{A}) + \text{N}_2(\text{A}) \rightarrow \text{N}_2(\text{C}) + \text{N}_2(\text{X})$	1.5×10^{-16}
R29. $\text{N}_2(\text{A}) + \text{O}_2(\text{X}) \rightarrow \text{N}_2(\text{X}) + \text{O}_2(\text{X})$	$8.75 \times 10^{-19} (T/300)^{0.55}$
R30. $\text{N}_2(\text{A}) + \text{O}_2(\text{X}) \rightarrow \text{N}_2(\text{X}) + \text{O}(^3\text{P}) + \text{O}(^3\text{P})$	$1.63 \times 10^{-18} (T/300)^{0.55}$
R31. $\text{N}_2(\text{A}) + \text{O}(^3\text{P}) \rightarrow \text{N}_2(\text{X}) + \text{O}(^3\text{P})$	2.1×10^{-17}
R32. $\text{N}(^4\text{S}) + \text{O}_2(\text{X}) \rightarrow \text{NO}(\text{X}) + \text{O}(^3\text{P})$	$1.1 \times 10^{-20} T \exp(-3150/T)$
R33. $\text{N}(^4\text{S}) + \text{O}_2(\text{a}) \rightarrow \text{NO}(\text{X}) + \text{O}(^3\text{P})$	$2.1 \times 10^{-20} \exp(-600/T)$
R34. $\text{N}_2(\text{B}) + \text{NO} \rightarrow \text{N}_2(\text{A}) + \text{NO}$	2.4×10^{-16}
R35. $\text{N}_2(\text{A}) + \text{NO}(\text{X}) \rightarrow \text{N}_2(\text{X}) + \text{NO}(\text{A})$	6.6×10^{-17}
R36. $\text{N}(^4\text{S}) + \text{O}(^3\text{P}) + \text{O}_2(\text{N}_2, \text{Ar}) \rightarrow \text{NO}(\text{X}) + \text{O}_2(\text{N}_2, \text{Ar})$	$1.76 \times 10^{-43} T^{-0.5}$
R37. $\text{N}(^4\text{S}) + \text{O}(^3\text{P}) + \text{O}_2(\text{N}_2, \text{Ar}) \rightarrow \text{NO}(\text{B}) + \text{O}_2(\text{N}_2, \text{Ar})$	$3.09 \times 10^{-46} (T/300)^{-1.4}$
R38. $\text{N}(^4\text{S}) + \text{O}(^3\text{P}) + \text{O}_2(\text{N}_2, \text{Ar}) \rightarrow \text{NO}(\text{A}) + \text{O}_2(\text{N}_2, \text{Ar})$	$2.12 \times 10^{-46} (T/300)^{-1.24}$
R39. $\text{N}(^4\text{S}) + \text{O}(^3\text{P}) \rightarrow \text{NO}(\text{A})$	$1.18 \times 10^{-23} (T/300)^{-0.35}$
R40. $\text{NO}(\text{A}) \rightarrow \text{NO}(\text{X}) + h\nu$	4.5×10^6
R41. $\text{NO}(\text{A}) + \text{N}_2 \rightarrow \text{NO}(\text{X}) + \text{N}_2$	1×10^{-19}
R42. $\text{NO}(\text{A}) + \text{O}_2 \rightarrow \text{NO}(\text{X}) + \text{O}_2$	1.5×10^{-16}
R43. $\text{NO}(\text{A}) + \text{NO} \rightarrow \text{NO}(\text{X}) + \text{NO}$	2×10^{-16}
R44. $\text{NO}(\text{B}) \rightarrow \text{NO}(\text{X}) + h\nu$	3×10^5
R45. $\text{NO}(\text{B}) + \text{N}_2 \rightarrow \text{NO}(\text{X}) + \text{N}_2$	6.1×10^{-19}
R46. $\text{NO}(\text{B}) + \text{O}_2 \rightarrow \text{NO}(\text{X}) + \text{O}_2$	1.5×10^{-17}
R47. $\text{NO}(\text{B}) + \text{NO} \rightarrow \text{NO}(\text{X}) + \text{NO}$	2×10^{-16}
R48. $\text{N}(^4\text{S}) + \text{NO} \rightarrow \text{O}(^3\text{P}) + \text{N}_2(\text{X}, v = 3)$	$1.05 \times 10^{-18} T^{0.5}$
R49. $\text{O}_2(\text{a}) + \text{NO} \rightarrow \text{O}_2(\text{X}) + \text{NO}$	2.5×10^{-23}
R50. $\text{O}_2(\text{b}) + \text{NO} \rightarrow \text{O}_2(\text{a}) + \text{NO}$	6×10^{-20}
R51. $\text{O}_2(\text{b}) + \text{N}_2 \rightarrow \text{O}_2(\text{a}) + \text{N}_2$	$1.7 \times 10^{-21} (T/300)$
R52. $\text{NO}(\text{X}) + \text{O}_3 \rightarrow \text{NO}_2(\text{X}) + \text{O}_2(\text{X})$	$4.3 \times 10^{-18} \exp(-1560/T)$
R53. $\text{O}(^3\text{P}) + \text{O}_2(\text{X}) + \text{N}_2 \rightarrow \text{O}_3 + \text{N}_2$	$5.7 \times 10^{-46} (300/T)^{2.8}$
R54. $\text{O}(^3\text{P}) + \text{NO}(\text{X}) + \text{N}_2(\text{Ar}) \rightarrow \text{NO}_2(\text{X}) + \text{N}_2(\text{Ar})$	1×10^{-43}
R55. $\text{O}(^3\text{P}) + \text{NO}(\text{X}) + \text{O}_2 \rightarrow \text{NO}_2(\text{X}) + \text{O}_2$	8.6×10^{-44}
R56. $\text{NO}(\text{X}) + \text{O}(^3\text{P}) + \text{N}_2 \rightarrow \text{NO}_2(\text{A}) + \text{N}_2 \rightarrow \text{NO}_2(\text{X}) + \text{N}_2$	3.7×10^{-44}
R57. $\text{NO}(\text{X}) + \text{O}(^3\text{P}) + \text{O}_2 \rightarrow \text{NO}_2(\text{A}) + \text{O}_2 \rightarrow \text{NO}_2(\text{X}) + \text{O}_2$	3.7×10^{-44}
R58. $\text{N}(^4\text{S}) + \text{NO}_2(\text{X}) \rightarrow \text{N}_2(\text{X}) + \text{O}_2(\text{X})$	7×10^{-19}
R59. $\text{N}(^4\text{S}) + \text{NO}_2(\text{X}) \rightarrow \text{NO}(\text{X}) + \text{NO}(\text{X})$	2.3×10^{-18}
R60. $\text{N}(^4\text{S}) + \text{NO}_2(\text{X}) \rightarrow \text{N}_2(\text{X}) + \text{O}(^3\text{P}) + \text{O}(^3\text{P})$	9.1×10^{-19}
R61. $\text{NO}_2(\text{X}) + \text{O}(^3\text{P}) \rightarrow \text{NO}(\text{X}) + \text{O}_2(\text{X})$	9.7×10^{-18}

creation when $|S_{\text{N}}^{\text{S}}| < |S_{\text{O}}^{\text{S}}|$ are

$$S_{\text{N}}^{\text{S}} = -\gamma_{\text{N}} \frac{v_{\text{N}}}{4} [\text{N}]; \quad (7)$$

$$S_{\text{O}}^{\text{S}} = -\gamma_{\text{O}} \frac{v_{\text{O}}}{4} [\text{O}]; \quad (8)$$

$$S_{\text{NO}}^{\text{S}} = \alpha(-S_{\text{N}}^{\text{S}}); \quad (9)$$

$$S_{\text{N}_2}^{\text{S}} = \frac{1}{2}(1 - \alpha)(-S_{\text{N}}^{\text{S}}); \quad (10)$$

$$S_{\text{O}_2}^{\text{S}} = \frac{1}{2}(-S_{\text{O}}^{\text{S}}) - \frac{1}{2}\alpha(-S_{\text{N}}^{\text{S}}). \quad (11)$$

In the reverse case the NO source is defined by the O atoms loss term S_{O}^{S} according to equation (9), while $S_{\text{O}_2}^{\text{S}}$ will have the form of $S_{\text{N}_2}^{\text{S}}$ from equation (10), and vice versa, with the proper interchange of S_{N}^{S} and S_{O}^{S} sources. During the investigations, by choosing α in the range 0.5–1 the effect of the NO surface production on the NO volume density distribution will be evaluated.

The recombination of atomic species on the surface depends on many parameters that can change from one experimental condition to another, e.g. surface material purity, cleanliness, morphology [27], oxide or nitride type [28], surface temperature [28–31], surface coverage [30], plasma environment—mixture composition [30, 32, 33]; therefore, it is very difficult to define a proper surface recombination coefficient for atoms (γ) when it comes to modelling of a given experimental condition [12, 26, 32, 34]. Thus in several models γ is used as a fitting parameter in order for the calculated densities to fit the measured values [34, 35].

In the literature can be found numerous works dealing with the determination of the surface recombination probabilities of atoms for different materials; however, there is quite a large discrepancy, such as orders of magnitude, between the results obtained by different authors. The source of these large differences between the data, as well as the effect of the variation of the surface recombination on the species densities,

Table 3. Measured N and O atoms surface recombination coefficients on stainless steel surface.

Recombination coefficient	Conditions	Reference
7.5×10^{-3}	<i>N-atoms</i> 1 Torr N ₂ pulsed RF discharge, $T_g = 300$ K	Adams <i>et al</i> [36]
$7 \times 10^{-2} \pm 0.02$	10–30 mTorr N ₂ RF discharge, $T_s = 320$ –340 K	Singh <i>et al</i> [37]
7×10^{-2}	<i>O-atoms</i> 0.5 mbar O ₂ flowing afterglow, $T_s = 300$ K	Mozetic <i>et al</i> [38]
2×10^{-2}	0.5 Torr O ₂ RF discharge, $T_s = 400$ –600 K	Gomez <i>et al</i> [39]
$1.7 \times 10^{-1} \pm 0.02$	10–30 mTorr O ₂ RF discharge, $T_s = 320$ –340 K	Singh <i>et al</i> [37]

has been discussed in detail in [26]. Table 3 shows the data found in the literature for the surface recombination coefficient of N and O atoms on the stainless steel surface. Here we can observe the order of magnitude differences between γ determined under different discharge conditions. In the case of N atoms, we use the results of [33] along with the results of Adams *et al* [36] determined at 1 Torr N₂, a condition closer to ours, and choose $\gamma_N = 7.5 \times 10^{-2}$, since it has been shown that in the case of metal surfaces the recombination probability of N atoms can increase one order of magnitude when a small amount, such as 0.1% O₂, is added to N₂ [33]. In the case of O atoms we choose $\gamma_O = 7 \times 10^{-2}$ determined by Mozetic *et al* [38] at 0.5 mbar in afterglow.

Here we would like to note that through surface processes the creation of NO₂ and N₂O molecules is also possible. The N₂O molecules can be created due to the re-association of the adsorbed NO molecules and N atoms on the surface ($\text{NO}_{(\text{ads})} + \text{N}_{(\text{ads})} \rightarrow \text{N}_2\text{O}_{(\text{ads})}$), as well as of two adsorbed NO molecules ($\text{NO}_{(\text{ads})} + \text{NO}_{(\text{ads})} \rightarrow (\text{NO})_{2(\text{ads})} \rightarrow \text{N}_2\text{O}_{(\text{ads})} + \text{O}_{(\text{ads})}$) [41]. According to Kline *et al* [42], N₂O can also be created through the $\text{N}_2 + \text{O}_{(\text{ads})} \rightarrow \text{N}_2\text{O}_{(\text{ads})}$ process. The surface production of NO₂ molecules is attributed to the re-association of adsorbed NO molecules with O atoms ($\text{NO}_{(\text{ads})} + \text{O}_{(\text{ads})} \rightarrow \text{NO}_{2(\text{ads})}$) [41]. The rates of these processes are mostly unknown, as well as the exact density of adsorbed species on the surface in the case of a stainless steel surface, as discussed in the previous paragraphs. The calculation of molecules production through these processes would be possible only with a very detailed surface model, which also implies the knowledge of the structure of the surface. Therefore, in this study we focus only on the surface production of the NO molecules, determining how the surface sources can influence the density distribution in the whole reactor.

Regarding the energy conservation equation we need as input data the temperature values at the inlet and on the boundary surfaces. The inlet temperature of the Ar⁺ ions is taken 12 000 K according to Selezneva *et al* [19], while the inlet O₂ and N₂ temperatures are chosen 300 K, and further the wall temperature is assumed to be 300 K [19].

Finally, our model is solved by using the algorithm given by Ferziger and Perić [43]. The equations are discretized using the finite volume method. The linear algebraic equation system so obtained is then solved with Stone's method iteratively using the multigrid method. In our solution three grid levels are used, the finest grid has $80 \times 40 \times 80$ control volumes.

4. Results and discussion

The three-dimensional model presented above is used to determine the expansion of the Ar⁺ jet in the reactor, to calculate the gas temperature distribution and the density distribution of different species created in the reactor.

First we investigate the evolution of the gas flow velocities and gas temperature in the reactor by comparing two different cases concerning the inlet velocity of the Ar⁺ ions: (i) $u(\text{Ar}^+) = 2000 \text{ m s}^{-1}$ and (ii) $u(\text{Ar}^+) = 3000 \text{ m s}^{-1}$. Here the inlet velocities of N₂ and O₂ injected into the reactor are chosen $w(\text{N}_2) = 20 \text{ m s}^{-1}$ and $w(\text{O}_2) = -100 \text{ m s}^{-1}$, respectively (corresponding to gas flow rates of 0.4 slm and 2 slm, respectively), while the total gas pressure in the reactor is kept at 0.2 Torr.

Figure 2(a) shows the distribution of the u velocity component in the x - z horizontal symmetry plane for the two cases. We note that for a clearer vision we have omitted from the figure the velocities below 40 m s^{-1} . The u component of the gas velocity, as shown by the figure, decreases one order of magnitude along the first 15 cm in the reactor, while it is strongly influenced by the w velocity component (initially that of N₂ and O₂), whose evolution in the reactor is depicted in figure 2(b). We can also observe that the expansion of the plasma is less influenced by the N₂ and O₂ injection when the Ar⁺ ions velocity is 3000 m s^{-1} .

In figure 2(c) we present the gas temperature distribution in the reactor. Here we can also observe the stronger influence of the 300 K O₂ and N₂ injected from the top and bottom, respectively, when the $u(\text{Ar}^+) = 2000 \text{ m s}^{-1}$. In this case the gas temperature at about 5 cm from the entrance reaches $\approx 2400 \text{ K}$ and $\approx 600 \text{ K}$ at the end of the reactor, while close to the other walls is $\approx 400 \text{ K}$. In the case of higher Ar⁺ ion velocity the temperature decreases more slowly in the reactor, in the right wall's vicinity temperatures as high as 700 K can be observed. The axial distribution of the, u , velocity and, T , temperature in the flow direction, $y = 12.5 \text{ cm}$ and $z = 12.5 \text{ cm}$, are presented in figures 2(e) and (f), respectively. Here the fast fall of the gas temperature during the first few centimetres, as well as that of the velocity can be seen more clearly. We note that we use a non-turbulent model and our axial resolution is 0.5 cm, thus we cannot describe accurately, from the point of view of gas dynamics, the turbulence occurring in the few centimetre zone around the entrance. We also note that the turbulence observed at the entrance vicinity [17, 19] does not influence the molecular kinetics. In this region the recombination of Ar⁺ ions (fast process) takes place due to their collision with N₂ and O₂ molecules, giving rise to N, O and Ar atoms.

The distribution of Ar atoms relative mass density is shown in figure 2(d). We can observe that after the short

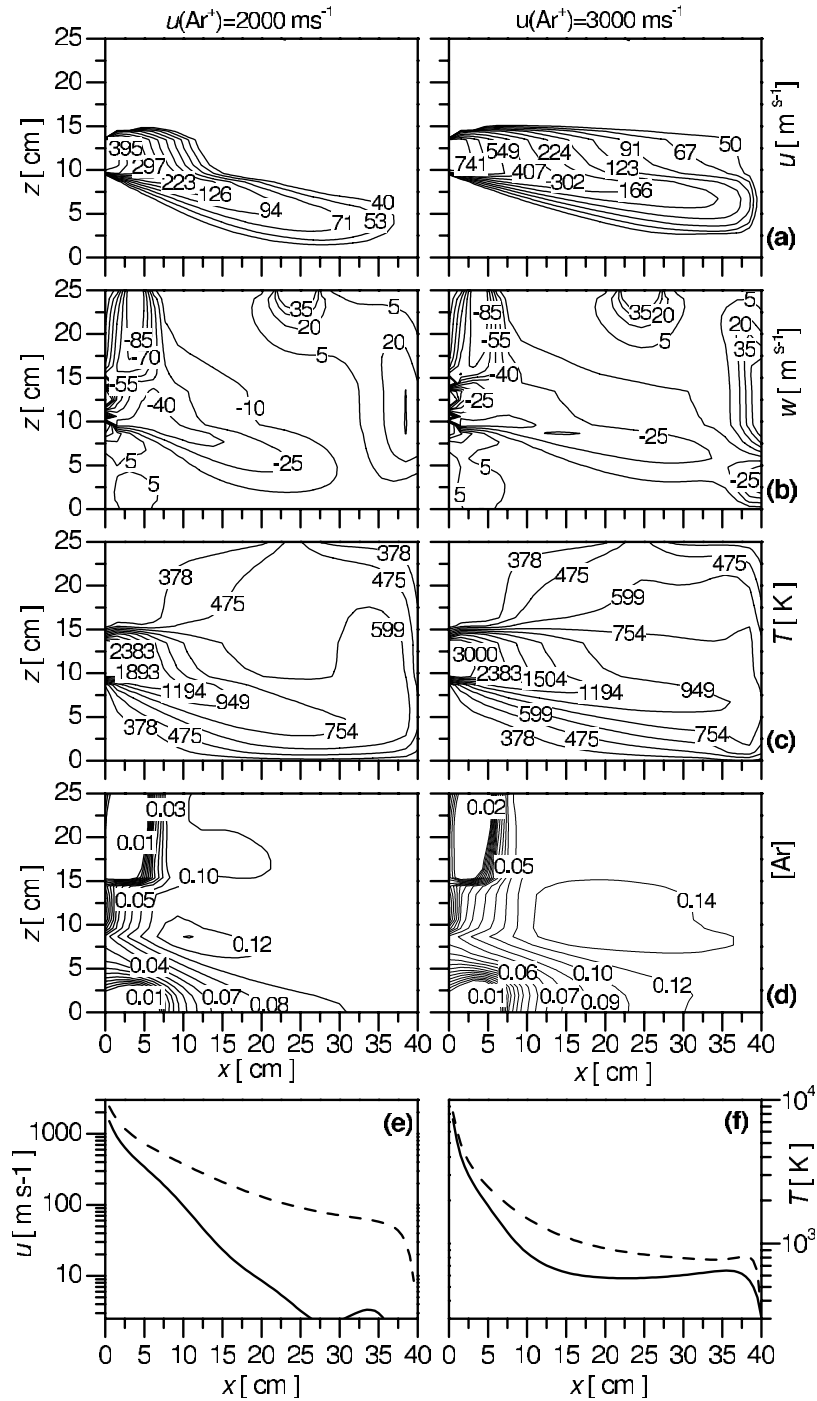


Figure 2. The distribution of velocities u (a) and w (b), of gas temperature (c) and of Ar atoms relative mass density (d) in the x - z vertical symmetry plane with $y = 12.5$ cm in the case of two different Ar^+ inlet velocities: 2000 m s^{-1} (first column) and 3000 m s^{-1} (second column). The axial distribution of u velocity (e) and of gas temperature (f) for $(y, z) = (12.5 \text{ cm}, 12.5 \text{ cm})$ in the case of $u(\text{Ar}^+) = 2000 \text{ m s}^{-1}$ (—) and $u(\text{Ar}^+) = 3000 \text{ m s}^{-1}$ (---).

recombination zone (slightly wider at the higher velocity) a homogeneous distribution of Ar atoms is obtained, the relative density of Ar is about 0.12 and 0.14, respectively. We note that the Ar^+ flux at the inlet $\rho \cdot u$ is $0.86 \text{ kg m}^{-2} \text{ s}^{-1}$ and $1.28 \text{ kg m}^{-2} \text{ s}^{-1}$ for $u(\text{Ar}^+) = 2000 \text{ m s}^{-1}$ and $u(\text{Ar}^+) = 3000 \text{ m s}^{-1}$, respectively, corresponding to $n \cdot u = 1.29 \times 10^{25} \text{ m}^{-2} \text{ s}^{-1}$ and $1.93 \times 10^{25} \text{ m}^{-2} \text{ s}^{-1}$, respectively.

In the following we study the creation of different species and their evolution in the reactor. The density

distributions are calculated for three different cases by changing the Ar^+ ions velocity and the flow of N_2 and O_2 as follows: (i) $u(\text{Ar}^+) = 2000 \text{ m s}^{-1}$, $w(\text{N}_2) = 20 \text{ m s}^{-1}$ and $w(\text{O}_2) = -60 \text{ m s}^{-1}$; (ii) $u(\text{Ar}^+) = 2000 \text{ m s}^{-1}$, $w(\text{N}_2) = 20 \text{ m s}^{-1}$ and $w(\text{O}_2) = -100 \text{ m s}^{-1}$; and (iii) $u(\text{Ar}^+) = 3000 \text{ m s}^{-1}$, $w(\text{N}_2) = 20 \text{ m s}^{-1}$ and $w(\text{O}_2) = -100 \text{ m s}^{-1}$.

As discussed in the model part (section 3, 3rd paragraph) the Ar^+ ions dissociate N_2 giving rise to $\text{N}^+(\text{S})$ atoms. These

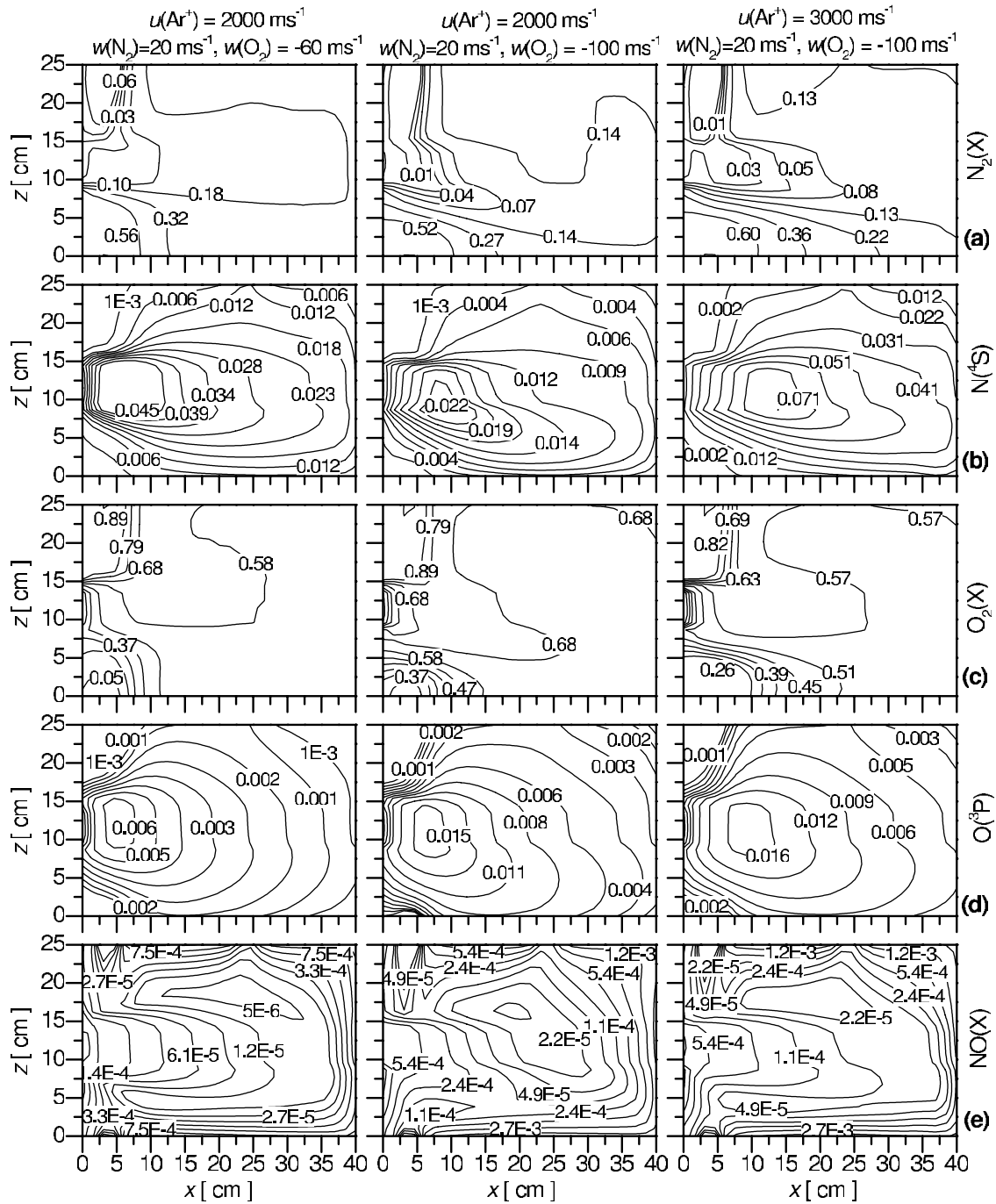


Figure 3. Relative density distributions, in the x - z vertical plane at $y = 12.5$ cm, for the following species: (a) $N_2(X)$, (b) $N(^4S)$, (c) $O_2(X)$, (d) $O(^3P)$ and (e) $NO(X)$. Columns 1–3 are for different inlet ion and molecular gas velocities.

N atoms in the reactor can recombine resulting in $N_2(B)$ molecules (R21 from table 2), and in collision with $O_2(X)$ produce $NO(X)$ molecules and $O(^3P)$ atoms (R32). The density distributions of N_2 molecules and $N(^4S)$ atoms in the x - z symmetry plane are shown in figures 3(a) and (b), respectively, for the above described three cases. As we could observe on the Ar atoms density distribution, the recombination of Ar^+ ions, thus the dissociation of N_2 molecules, occurs along the first 10 cm in the reactor, and as a consequence a quite homogeneous N_2 density distribution builds up in the remaining part of the reactor. At higher

Ar^+ ions velocity, however, this homogeneous part is more restricted, as can be seen in the third column of the figure. The dissociation of N_2 , however, is influenced by the O_2 gas flow, since there are two competing reactions in the system, the dissociation of N_2 and O_2 molecules, respectively. The N atoms density distribution (figure 3(b)) shows that depending on the Ar^+ ions velocity and molecular gas flows, relative densities between 10^{-3} and 7×10^{-2} have been obtained, and further, by adjusting the molecular gas flow rates different dissociation degrees can be achieved. Since in the reactor the N atoms kinetics is governed by recombination processes

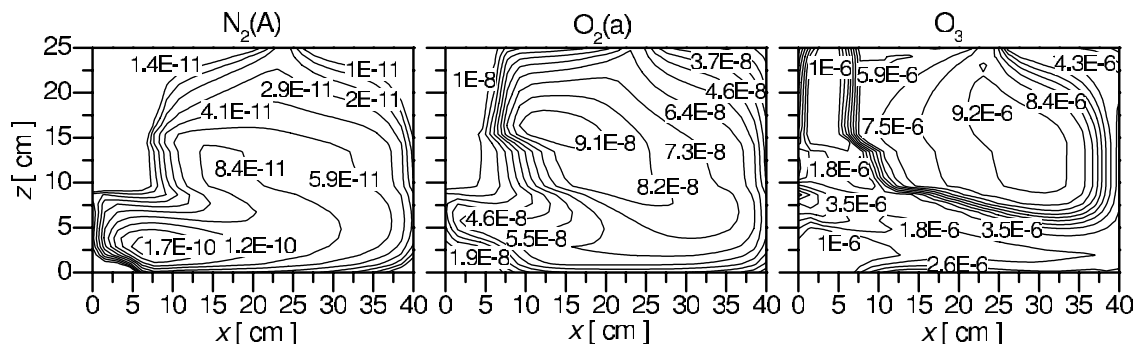


Figure 4. Relative density distributions, in the x - z vertical plane at $y = 12.5$ cm, for $N_2(A)$, $O_2(a)$ and O_3 in the case of $u(\text{Ar}^+) = 2000$ m s $^{-1}$, $w(N_2) = 20$ m s $^{-1}$ and $w(O_2) = -100$ m s $^{-1}$.

(e.g. R21, R32, R36–R38, R48) the N atoms densities, as shown on the density distributions, decrease to the walls. The N atoms density decrease can be up to one order of magnitude in the reactor. The N atoms in the gas phase can recombine into $N_2(B)$ molecules (R21), which consecutively, through radiation transfer and quenching (R22, R24), turn into $N_2(A)$ metastable molecules. The relative density of $N_2(A)$ metastable in the reactor is between 10^{-11} and 10^{-10} , while that of $N_2(B)$ molecules is about 2 orders of magnitude lower, but has similar distribution as $N_2(A)$. The $N_2(A)$ density distribution is shown in figure 4 for case (ii).

Figures 3(c) and (d) show the density distributions of $O_2(X)$ and $O(^3P)$ atoms. Since the O_2 gas flow has been set two and five times, respectively, higher than that of N_2 gas, correspondingly higher $O_2(X)$ molecular densities are obtained in the reactor. Even though the O_2 gas flow is much higher than that of N_2 , the $O(^3P)$ atoms density is lower than that of $N(^4S)$ in the reactor, since the O_2 is less efficiently dissociated than N_2 . This result shows the main difference between this system and the afterglow of an N_2 - O_2 discharge, where the O_2 molecules are mostly dissociated even in the case of low O_2 percentage in the gas mixture, while the N_2 dissociation is just a few per cent [10, 11, 40, 44]. In contrast to N_2 - O_2 discharges, here the dissociation processes are governed only by the Ar^+ recombination dissociation. As a consequence, in this system the N and O atoms density ratio could be varied in a wide range by adjusting the N_2 and O_2 inlet gas flow rates.

The $O(^3P)$ atoms losses in the reactor are governed by three-body gas phase recombination processes (R1–R6, R17 in table 1, R36–R38) and by atomic surface recombination on the reactor's wall. The $O(^3P)$ atoms in collision with $O(^3P)$ and $O_2(X)$ (R2–R6) give rise to $O_2(a)$, $O_2(b)$ and O_3 molecules. The relative densities obtained for $O_2(a)$ and $O_2(b)$ in the reactor are between 10^{-8} and 10^{-7} , with the maximum in the middle of the reactor. The density distribution of $O_2(a)$ is shown in figure 4 for case (ii), the $O_2(b)$ density distribution shows the same features. In the case of O_3 relative densities between 10^{-6} and 10^{-5} have been observed, see figure 4.

As discussed in the model part (section 3) the N and O atoms on the surface can recombine into N_2 and O_2 , respectively, and NO molecules. The present calculations have been conducted by taking the atomic surface recombination

coefficients $\gamma_N = 7.5 \times 10^{-2}$ and $\gamma_O = 7 \times 10^{-2}$ and assuming that 50% ($\alpha = 0.5$) of the atoms recombined on the surface result into NO. Figure 3(e) shows the density distribution of NO(X) molecules in the reactor. The calculations show that the surface production of NO dominates over the gas phase production, since the highest NO(X) densities occur near the surface, here relative densities as high as 2×10^{-3} are obtained. In the gas phase the limiting factor for NO production is the $O_2(X)$ and O atoms density. As calculations show with the increase in the O_2 gas flow, consequently increase in O atoms density, the NO(X) density in the bulk of the reactor also increases significantly. However, the density of NO(X) is also strongly influenced by the loss processes, the collision of NO(X) with N atoms (R48), present with high density in the reactor, results in $O(^3P)$ and $N_2(X)$. The NO(X) molecules in the reactor contribute to the formation of $NO_2(X)$ molecules (R54–R57 table 2), whose distribution shows similar features to that of NO(X) with relative densities values between 10^{-9} and 10^{-7} .

The $N(^4S)$ and $O(^3P)$ atoms also contribute to the production of UV emitting NO(A) and NO(B) molecules, which are both created through the three-body re-association of N and O atoms implying N_2 , O_2 or Ar as the third body [13] (R37–R38). Since we work at rather low pressure, the production of excited NO(A) and NO(B) molecules through the three-body processes is quite low. Their relative densities in the reactor are in the range of 10^{-12} , and due to the decrease in atomic species in the reactor the NO(A) and NO(B) densities decrease strongly to the walls. As a consequence, the intensity of the UV radiation due to NO(A) and NO(B) radiative deexcitation is very low. At the higher investigated gas flows, case (iii), photon fluxes of 5×10^{10} cm $^{-3}$ s $^{-1}$ can be expected. If we aim for stronger UV radiation, higher gas pressure should be adjusted. In comparison with the N_2 - O_2 discharges, while there the NO(A) and NO(B) densities are limited by the $N(^4S)$ atoms density, here it is influenced by the lower $O(^3P)$ densities.

As already mentioned, the presented above results have been calculated assuming $\gamma_N = 7.5 \times 10^{-2}$ and $\gamma_O = 7 \times 10^{-2}$; however, as already discussed, the exact determination of the atomic surface recombination probability for a given experimental condition is very difficult. The surface recombination probability of atoms depends on the mixture

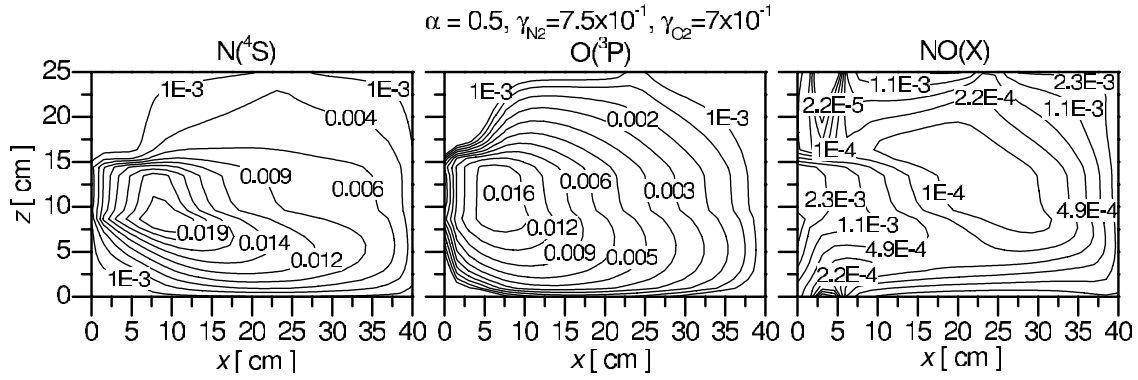


Figure 5. Density distribution of $N(^4S)$, $O(^3P)$ and $NO(X)$ in the x - z vertical symmetry plane when $\gamma_N = 7.5 \times 10^{-1}$ and $\gamma_O = 7 \times 10^{-1}$ in the case of $u(Ar^+) = 2000 \text{ m s}^{-1}$, $w(N_2) = 20 \text{ m s}^{-1}$ and $w(O_2) = -100 \text{ m s}^{-1}$.

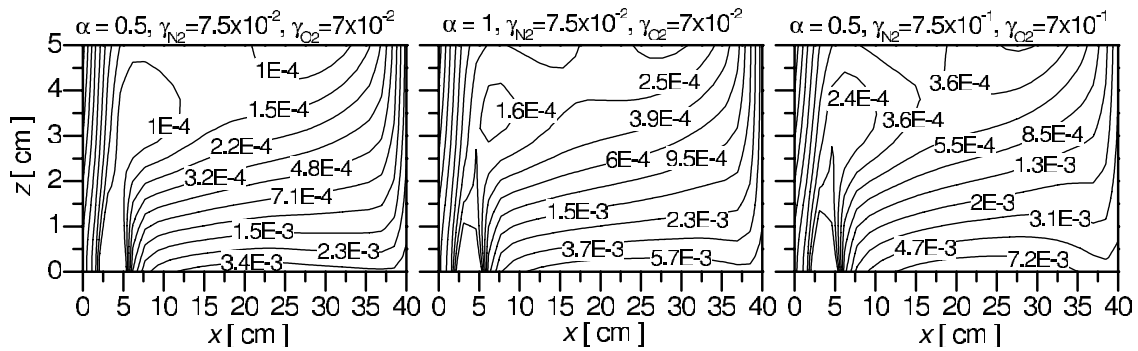


Figure 6. Density distribution of $NO(X)$ in the x - z vertical plane at $y = 12.5 \text{ cm}$ with the z coordinate varying only in the 0–5 cm interval. The distributions are shown for different assumed α and γ values.

composition, but also on the gas pressure and the temperature, namely increases with decreasing pressure and with increasing gas and wall temperature. In the following we investigate the effect of the higher atomic surface recombination probability on the atomic and molecular densities. Figure 5 shows the density distributions in the x - z vertical symmetry plane when $\gamma_N = 7.5 \times 10^{-1}$ and $\gamma_O = 7 \times 10^{-1}$ in the case of $u(Ar^+) = 2000 \text{ m s}^{-1}$, $w(N_2) = 20 \text{ m s}^{-1}$ and $w(O_2) = -100 \text{ m s}^{-1}$. Compared with the densities obtained with the lower surface recombination probabilities, see second column of figure 3, the atomic densities decrease faster in the reactor reaching lower density values near the wall. In contrast, due to the more efficient atomic surface recombination, the $NO(X)$ density significantly increases in the reactor. Figure 6 shows the $NO(X)$ densities in the wall vicinity for three different cases: (i) $\alpha = 0.5$, $\gamma_N = 7.5 \times 10^{-2}$ and $\gamma_O = 7 \times 10^{-2}$; (ii) $\alpha = 1$, $\gamma_N = 7.5 \times 10^{-2}$ and $\gamma_O = 7 \times 10^{-2}$ and (iii) $\alpha = 0.5$, $\gamma_N = 7.5 \times 10^{-1}$ and $\gamma_O = 7 \times 10^{-1}$. The calculations show that by assuming $\alpha = 1$ instead of $\alpha = 0.5$, the $NO(X)$ density near the wall increases by about a factor of 2, while keeping $\alpha = 0.5$ and increasing the surface recombination coefficients by one order of magnitude it increases more than a factor of 2. We can conclude that in this system the $NO(X)$ density in the reactor is strongly influenced by the surface processes, namely the surface recombination of atoms, which is determined mainly by the state of the surface, which changes from one experimental system to the other [26].

5. Concluding remarks

We have investigated the expansion of a supersonic Ar^+ ion jet in a low pressure reactor filled with N_2 and O_2 . The velocity of Ar^+ ions has been chosen 2000 m s^{-1} and 3000 m s^{-1} , respectively, while the N_2 and O_2 have been injected into the reactor at flow rates of 0.4–2 slm. The investigations have been carried out with the help of a three-dimensional hydrodynamic model, which makes possible the determination of the velocities, temperature and species density distributions in the whole three-dimensional reactor. During the calculations we have determined the gas velocity fields and the temperature distributions for different flow conditions. We have shown that the molecular gas flow strongly influences the expansion of the jet and the temperature distribution of the gas.

We have studied the formation of different species through the molecular kinetics triggered by the collision of Ar^+ ions with N_2 and O_2 , by assuming that the ion induced dissociation happens in a single step. We have shown that the main difference between this system and an N_2 - O_2 post-discharge lies in the dissociation degrees of N_2 and O_2 . While in an N_2 - O_2 post-discharge the N_2 dissociation degree is low and that of O_2 is high, in the present system this can be varied through the gas flow rate of the molecular gases. Comparing with the post-discharge of an N_2 - O_2 surface wave microwave discharge [44], in this system the O_3 production is more efficient, densities order of magnitude higher can be achieved,

as well as for the NO(*X*) and N₂(*B*) molecules, while the density of O₂(*a*) metastables is orders of magnitude lower.

We concluded that the NO(*X*) molecules formation is governed by the surface processes, which is strongly influenced by the state of the surface.

Acknowledgments

The work has been supported by the Hungarian Science Foundation OTKA, through project F-67556 and by Janos Bolyai Research Scholarship of the Hungarian Academy of Sciences. The authors gratefully acknowledge Vasco Guerra for several fruitful discussions.

References

- [1] Gaillard M, Raynaud P and Ricard A 1999 *Plasma Polym.* **4** 241
- [2] Moreau S *et al* 2000 *J. Appl. Phys.* **88** 1166
- [3] Ricard A and Monna V 2002 *Plasma Sources Sci. Technol.* **11** 1
- [4] Lin T H, Belser M and Tzeng Y 1988 *IEEE Trans. Plasma Sci.* **16** 631
- [5] Hody V *et al* 2006 *Thin Solid Films* **506–507** 212
- [6] Yasuda Y, Zaima S, Kaida T and Koide Y 1990 *J. Appl. Phys.* **67** 2603
- [7] Barnes T M *et al* 2004 *J. Appl. Phys.* **96** 7036
- [8] Sage D, Espuche E and Soulier J-P 1999 *Le Vide* **54** 429
- [9] Canal C, Gaboriau F, Molina R, Erra P and Ricard A 2007 *Plasma Process. Polym.* **4** 445
- [10] Merel P, Tabbal M, Chaker M, Moisan M and Ricard A 1998 *Plasma Sources Sci. Technol.* **7** 550
- [11] Guerra V and Loureiro J 1995 *J. Phys. D: Appl. Phys.* **28** 1903
- [12] Pintassilgo C D, Loureiro J and Guerra V 2005 *J. Phys. D: Appl. Phys.* **38** 417
- [13] Kutasi K, Saoudi B, Pintassilgo C D, Loureiro J and Moisan M 2008 *Plasma Process. Polym.* **5** 840
- [14] Kutasi K, Pintassilgo C D and Loureiro J 2009 *J. Phys.: Conf. Ser.* **162** 012008
- [15] van Helden J H, Zijlmans R A B, Schram D C and Engeln R 2009 *Plasma Sources Sci. Technol.* **18** 025020
- [16] Zijlmans R, Welzel S, Gabriel O, van Helden J H, Röpcke J, Schram D C and Engeln R 2008 *Publ. Astron. Obs. Belgrade* **84** 148
- [17] Engeln R, Mazouffre S, Vankan P, Schram D C and Sadeghi N 2001 *Plasma Sources Sci. Technol.* **10** 595
- [18] van de Sanden M C M, Severens R J, Kessels W M M, Meulenbroeks R F G and Schram D C 1998 *J. Appl. Phys.* **84** 2427
- [19] Selezneva S E, Boulos M I, van de Sanden M C M, Engeln R and Schram D C 2002 *J. Phys. D: Appl. Phys.* **35** 1362
- [20] Kutasi K, Pintassilgo C D, Coelho P J and Loureiro J 2006 *J. Phys. D: Appl. Phys.* **39** 3978
- [21] Belmonte T, Czerwiec T, Gavillet J and Michel H 1997 *Surf. Coat. Technol.* **97** 642
- [22] Viaggiano A A and Morris R A 1993 *J. Chem. Phys.* **99** 3526
- [23] Midey A J and Viggiano A A 1998 *J. Chem. Phys.* **109** 5257
- [24] Guerra V and Loureiro J 1999 *Plasma Sources Sci. Technol.* **8** 110
- [25] Kim Y C and Boudart M 1991 *Langmuir* **7** 2999
- [26] Kutasi K and Loureiro J 2007 *J. Phys. D: Appl. Phys.* **40** 5612
- [27] Cvelbar U and Mozetič M 2007 *J. Phys. D: Appl. Phys.* **40** 2300
- [28] Lefevre L, Belmonte T, Czerwiec T, Ricard A and Michel H 1999 *Surf. Coat. Technol.* **116–119** 1244
- [29] Macko P, Veis P and Cernogora G S 2004 *Plasma Sources Sci. Technol.* **13** 251
- [30] Nasuti F, Barbato M and Bruno C 1996 *J. Thermophys. Heat Transfer*
- [31] Pagnon D, Amorim J, Nahorny J, Touzeau M and Vialle M 1995 *J. Phys. D: Appl. Phys.* **28** 1856
- [32] Gordiets B, Ferreira C M, Nahorny J, Pagnon D, Touzeau M and Vialle M 1996 *J. Phys. D: Appl. Phys.* **29** 1021
- [33] Marković V Lj, Petrović Z Lj and Pejović M M 1995 *Japan. J. Appl. Phys.* **34** 2466
- [34] Pinheiro M J, Gousset G, Granier A and Ferreira C M 1998 *Plasma Sources Sci. Technol.* **7** 524
- [35] Gordiets B, Ferreira C M, Guerra V, Loureiro J, Nahorny J, Pagnon D, Touzeau M and Vialle M 1995 *IEEE Trans. Plasma Sci.* **23** 750
- [36] Adams S F and Miller T A 2000 *Plasma Sources Sci. Technol.* **9** 1
- [37] Singh H, Coburn J W and Graves D B 2000 *J. Appl. Phys.* **88** 3748
- [38] Mozetič M and Zalar A 2000 *Appl. Surf. Sci.* **158** 263
- [39] Gomez S, Steen P G and Graham W G 2002 *Appl. Phys. Lett.* **81** 19
- [40] Mozetic M, Ricard A, Levaton J, Monna V, Babic D, Poberaj I and Cvelbar U 2003 *J. Vac. Sci. Technol. A* **21** 369
- [41] Burch R, Daniells S T and Hu P 2002 *J. Chem. Phys.* **117** 2902
- [42] Kline L, Partlow W D, Young R M, Mitchell R R and Congedo T V 1991 *IEEE Trans. Plasma Sci.* **19** 278
- [43] Ferziger J H and Peric M 2002 *Computational Methods for Fluid Dynamics* 3rd revised edn (Berlin: Springer)
- [44] Kutasi K, Pintassilgo C D, Loureiro J and Coelho P J 2007 *J. Phys. D: Appl. Phys.* **40** 1990